

Nuclear spin dynamics and magnetic structure of nanosized particles of $\text{La}_{0.7}\text{Sr}_{0.3}\text{MnO}_3$

M. M. Savosta, V. N. Krivoruchko, I. A. Danilenko, V. Yu. Tarenkov, T. E. Konstantinova, A. V. Borodin, and V. N. Varyukhin
Donetsk Physics & Technology Institute NASU, R. Luxemburg 72, 83114 Donetsk-114, Ukraine

(Received 6 August 2003; published 23 January 2004)

Detailed studies of both ^{55}Mn NMR spectra and nuclear relaxation, completed by magnetic measurements, have been performed to obtain microscopic information on the magnetic structure of fine scale (~ 50 and ~ 100 – 200 nm) particles of $\text{La}_{0.7}\text{Sr}_{0.3}\text{MnO}_3$ prepared by the coprecipitation method. Measurements of the resistance and magnetoresistance have also been carried out to assist these data. Our results on nuclear spin dynamics provide direct evidence of previous statements that a grain boundary in magnetoresistive manganites is not a magnetically and electrically sharp interface but should be considered as a transfer region of several monolayers different from the grain's inner part magnetic and structure orders.

DOI: 10.1103/PhysRevB.69.024413

PACS number(s): 75.75.+a, 75.47.Gk, 75.30.-m

I. INTRODUCTION

Magnetic properties of manganites at the nanometer scale comprise an issue of great interest nowadays. A number of investigations of the grain size effect on magnetotransport or magnetic properties of perovskites $\text{La}_{1-x}\text{A}_x\text{MnO}_3$ have been published recently (see, e.g., Refs. 1–13). In particular, with regard to colossal magnetoresistive properties of manganites, spin electronics based on half-metallic properties of these materials, etc., the surface spin and structure disorders and their possible influence on the magnetism of manganite nanoparticles are matters of intense discussion. The following draft picture for a grain-boundary magnetic structure has emerged at present: since the double exchange mechanism is sensitive to a Mn-O-Mn bound state, any structural disorder near the grain boundary (oxygen non-stoichiometry, vacancies, stress, etc.) modifies this exchange and leads to a spin disorder. Due to a strong Hund's interaction, spin disorder around grain boundaries serves as a strong scattering center for highly spin-polarized conduction electrons and results in a high zero-field electrical resistance. The application of a moderate magnetic field can align the originally disordered Mn spins, thus reducing the scattering and leading to a giant magnetoresistance. However, so far the microscopic nature of the surface region is not well understood. This lack of understanding is manifested in some inconsistency between the models and the experimental results. For example, it has been assumed that the grain surface magnetization is suppressed compared to the bulk magnetization;^{2,4} meanwhile, the Curie temperature near the grain boundary was found to be enhanced;⁷ some authors found a shift of the chemical potential between the external region and the inner part of the grain;^{6,10} others suggest a high probability of tunneling through paramagnetic impurity states in the intergranular barrier,^{4,5,9} etc. The recognition and elucidation of the grain size effect is crucial if manganites are expected to be used in forthcoming micro-electronic devices.

Nuclear magnetic resonance (NMR) is a suitable microscopic tool to provide further insight into the problem, because it probes locally different charge states and their dynamics. However, only ^{55}Mn NMR experiments on a series of $\text{La}_{2/3}\text{Ca}_{1/3}\text{MnO}_3$ thin films¹³ have been performed to date. Nuclear spin dynamics of nanosized manganites has not been

reported until now. In the present paper we report, for the first time to our best knowledge, detailed studies of both the NMR spectra and nuclear relaxation, completed by magnetic measurements, for nanosized $\text{La}_{0.7}\text{Sr}_{0.3}\text{MnO}_3$ powders obtained by the coprecipitation method. The results indicate that a nanoparticle's crystal and magnetic structures can be modeled by a structure where, at least on a scale of several monolayers, the M-O-Mn bound states near the grain surface are considerably different from those in bulk of the grain. The temperature dependencies of the resistance and magnetoresistance (MR) of nanocompact $\text{La}_{0.7}\text{Sr}_{0.3}\text{MnO}_3$, as well as break junctions (magnetoresistance of the $\text{La}_{0.7}\text{Sr}_{0.3}\text{MnO}_3/\text{La}_{0.7}\text{Sr}_{0.3}\text{MnO}_3$ interface) have also been investigated. Experimental results obtained from electrical transport properties support the model.

In Sec. II, we briefly describe the preparation and structural characteristics of the samples we are dealing with. Our results on macroscopic magnetic properties of compacted powders are presented in Sec. III. Section IV is the central one; here we present our extensive data on nuclear spin dynamics for nanosized grains of $\text{La}_{0.7}\text{Sr}_{0.3}\text{MnO}_3$. Transport properties will be discussed in Sec. V. In Sec. VI we summarize the results and formulate the main conclusions.

II. SAMPLES PREPARATION

We have selected the coprecipitation method as an alternative method to a solid-state reaction, mainly used for manganite bulk samples preparation. Our method allows one to have more accurate control of the sintering temperatures, as well as of the final particle size. For this study, the powder of $\text{La}_{0.7}\text{Sr}_{0.3}\text{MnO}_3$ was synthesized by the coprecipitation method supplemented by microwave heating and ultrasound treatment.¹⁴ During the first step of preparation stoichiometric amounts of $\text{La}(\text{NO}_3)_2$, $\text{SrCl}_2 \cdot 2\text{H}_2\text{O}$, $\text{Mn}(\text{NO}_3)_3 \cdot 6\text{H}_2\text{O}$ and $(\text{NH}_4)_2\text{CO}_3$ were dissolved in a liquid solution. All chemicals that were used in the synthesis procedure were reagent grade. A nanometer scaled $\text{La}_{0.7}\text{Sr}_{0.3}\text{MnO}_3$ powder was obtained directly by annealing the solution at 1000°C for 60 min. The precipitate was then washed several times in order to remove the by-products of the reaction. The hydrogel was dried in the thermo-box. Powders were dried in pulsed magnetic field at 120°C in a special setup with the

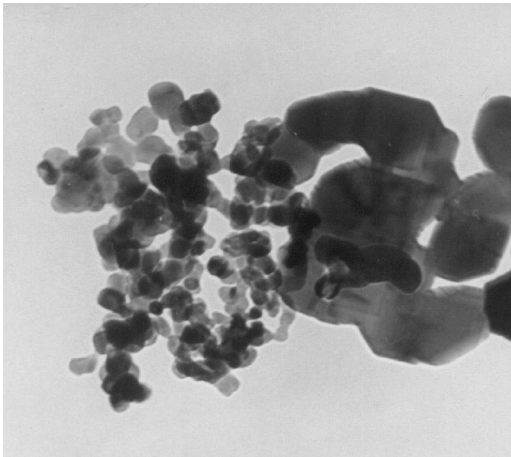


FIG. 1. TEM image of $\text{La}_{0.7}\text{Sr}_{0.3}\text{MnO}_3$ powder; larger particles have a size of $\sim 100\text{--}200$ nm; fine scale particles have a size of ~ 50 nm.

magnitude of magnetic field $H = 10^4\text{--}10^5$ A/m and frequency $f = 0.5\text{--}10$ Hz.

The phase structure of powdered and compacted samples was determined by x-ray diffraction, as well as by transmission and scanning electron microscopy. The $\text{La}_{0.7}\text{Sr}_{0.3}\text{MnO}_3$ patterns of pure rhombic perovskite structure were formed. However, using transmission electron microscopy (TEM), we found that the powder was characterized by grains of two morphology types (see Fig. 1): by particles of a relatively large size (100–200 nm) and a shape close to rectangular, and by fine scale (~ 50 nm) particles with an isometric shape. Our rough estimations give that about 50% of the powder weight is particles of one morphology type and 50% is of another. Both types of particles have the same TEM image which corresponds to the x-ray diffraction data. We suppose that the two types of particle morphology are due to the presence of two oxide phases on early stages of $\text{La}_{0.7}\text{Sr}_{0.3}\text{MnO}_3$ syntheses processes.

The volume of the powder we were working with was about 100 g. To examine the grain size effect, half of the powder was further annealed for 8 h at 1100°C . According to Ref. 14, this leads to an increase of the average grain size of the particles up to typical for ceramic systems values of about $1\ \mu\text{m}$. Powder before the annealing will be referred to below as sample 1, (S1), and the powder after being annealed as sample 2 (S2).

III. MAGNETIZATION

Magnetic properties were measured in Institute of Physics (Praga, Czech Republic) using a Quantum Design superconducting quantum interface device (SQUID) magnetometer in the temperature range from 5 to 400 K. In addition, our home-made equipment was used for the measurement of the initial ac susceptibility in between 77 and 400 K.

The temperature dependence of the samples S1 magnetization in the field-cooled (FC) process with an applied low magnetic field of 100 Oe is presented in Fig. 2 (solid line, left panel). At cooling, magnetization increases smoothly up

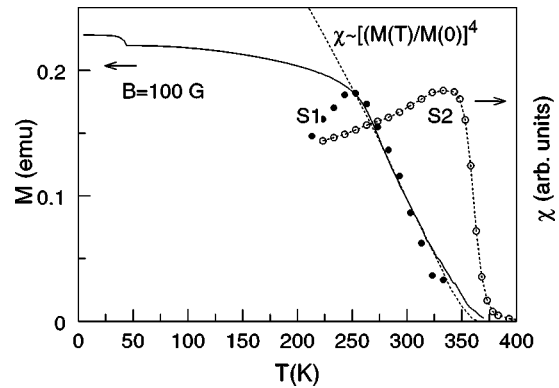


FIG. 2. Temperature dependence of low-field FC magnetization (solid curve) and ac susceptibility (\bullet) for a nanosized powder of $\text{La}_{0.7}\text{Sr}_{0.3}\text{MnO}_3$ (S1); and an ac susceptibility (\circ) of ceramic S2 samples of $\text{La}_{0.7}\text{Sr}_{0.3}\text{MnO}_3$.

to ~ 250 K, while below this temperature the FC curve becomes similar to that observed in the bulk material. A similar behavior with a maximum at 250 K is also observed for ac susceptibility (Fig. 2, dots, right panel). Remarkably, for Curie temperature, determined as the onset of magnetization, we find a value $T_C \approx 360$ K, which is close to that in a polycrystalline sample of the same composition.¹⁵ Besides, the behavior of magnetization ($H = 100$ Oe) and ac susceptibility for the S1 samples in between 365 and 250 K is well described by $[M(T)/M(0)]^4$ law (dashed curve on Fig. 2), where $M(T)$ dependence for polycrystalline sample is taken from Ref. 15. Note also, that the ferromagnetic-paramagnetic transition is substantially broader compared to that reported in Ref. 15, indicating that grain size still plays an important role. The sharp upturn in the magnetization curve below 44 K is probably due to the presence of a ferromagnetic phase of Mn_3O_4 in the amount of $\sim 7\%$ [Mn_3O_4 has $T_C = 42$ K and $\sigma = 42$ emu/g at 5 K (Ref. 16)]. Note that a similar increase in magnetization was also observed by Zhu *et al.*⁸ for nanosized $\text{La}_{2/3}\text{Sr}_{1/3}\text{MnO}_3$, but the authors attributed this feature to spin-glass freezing on surface of nanoparticles.

The ac susceptibility for the S2 samples is more conventional. The Curie temperature determined as the inflection point in the susceptibility curve, $T_C = 364$ K, is close to that observed in a similar polycrystalline sample.

IV. NMR EXPERIMENTS

The NMR spectra were recorded by the two-pulse spin echo method at temperatures between 77 and 310 K using a noncoherent spectrometer with a frequency sweep and box-car detector signal averaging. The NMR spectra were obtained by measuring the integrated intensity of the spin-echo versus frequency using $\tau = 3.5\ \mu\text{s}$, where τ is the time separation between the two pulses. The spin-echo intensities were corrected for the f^2 -type frequency response. The nuclear spin-spin relaxation was studied by measuring the spin-echo decay as a function of τ . We also probed the spin-lattice relaxation using the saturation-recovery method. It was found that in general the spin-lattice relaxation is slower by an order of magnitude than the spin-spin relaxation, and both

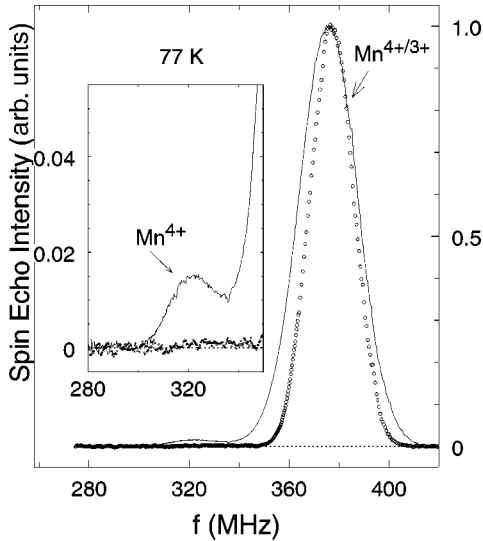


FIG. 3. ^{55}Mn NMR spectra recorded for S1 (solid line) and S2 (○) samples at 77 K. Inset: the same spectra on an expanded scale, showing the details of NMR spectra at about 320 MHz.

have similar temperature dependences. This situation was already discussed for (LaNa) manganites.¹⁷ Therefore, herein after we restrict our study of nuclear spin dynamics by considering the spin-spin relaxation only.

A. NMR spectra

The electronic moment of the ^{55}Mn ions is coupled to the nucleus via the hyperfine interaction, so that the Mn nucleus would experience, in a magnetically ordered state, a local field given by

$$^{55}\mathbf{B}_l = \hat{A}\mathbf{M}_l + \sum_i B_i\mathbf{M}_i + \mathbf{B}_0, \quad (1)$$

where the sum on the right hand side contains contributions from the on-site ($\hat{A}\mathbf{M}_l$), from the (six) magnetic nearest neighbors, and from the external magnetic field \mathbf{B}_0 to the hyperfine field; $\mathbf{M}_{l,i}$ is the averaged $\text{Mn}^{3+/4+}$ local magnetization. The hyperfine coupling \hat{A} in principle is a tensor of symmetry according to the point group, while B_i are of scalar nature. The resonance frequency f_{res} is related to local field by $f_{\text{res}} = \gamma|^{55}\mathbf{B}_l|/2\pi$, where $\gamma/2\pi = 10.6$ MHz/T for the ^{55}Mn nuclei. Equation (1) predicts separate resonance frequencies in the presence of nearest-neighbor vacancies, in the appearance of inequivalent Mn sites, if the local symmetry is lower than cubic, etc.

^{55}Mn NMR spectra of S1 and S2 samples at $T=77$ K are presented in Fig. 3. The dominant line at $f_{\text{res}}=377$ MHz is typical of mixed valence metalliclike manganites and corresponds to a fast hopping of electron holes among the Mn sites. When the hopping of electron holes is slower than the frequency splitting Δf of the Mn^{4+} and Mn^{3+} resonances, two distinct lines at $f_{\text{res}} \approx 315\text{--}332$ MHz and $f_{\text{res}} \approx 370\text{--}435$ MHz for Mn^{4+} and Mn^{3+} , respectively, are observed.^{18–20}

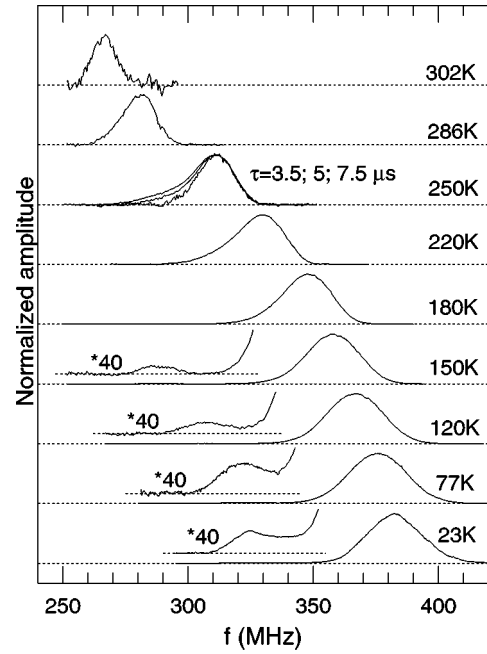


FIG. 4. Temperature dependence of ^{55}Mn NMR spectra in a nanosized sample. For $T=250$ K spectra taken for three different values of time interval τ between the exciting and refocusing pulses are shown.

Closer inspection of Fig. 3 (see the inset) reveals an additional relatively small contribution for the S1 sample at $f_{\text{res}}=321$ MHz, corresponding to Mn^{4+} states. The NMR signal corresponding to Mn^{3+} was not detected probably because of overlapping with strong $\text{Mn}^{3+/4+}$ signal and/or due to fast spin-spin relaxation. The line assigned to Mn^{4+} arises most likely from the surface of the nanoparticles since it is no longer observed for S2 samples. Notice that the Mn^{4+} NMR line was also detected in $\text{La}_{2/3}\text{Ca}_{1/3}\text{MnO}_3$ thin films.¹³ Another manifestation of the grain size effect on the NMR spectra consists of a much broader main line for S1 samples (solid line on Fig. 3, with a half-width $\Delta f_{1/2}=27$ MHz) compared to S2 samples (dotted line with a half-width $\Delta f_{1/2}=21$ MHz). It is interesting that for a ceramic sample studied in Ref. 15, the NMR line at 77 K is still a little narrower [$\Delta f_{1/2}=19(1)$ MHz].

The NMR spectra of $\text{La}_{0.7}\text{Sr}_{0.3}\text{MnO}_3$ nanoparticles at different temperatures are displayed in Fig. 4. The increase of temperature leads to a rapid, approximately exponential, decrease of the spin-spin relaxation time T_2 which is similar to other manganite systems.^{17,21} We were able to observe $\text{Mn}^{3+/4+}$ (Mn^{4+}) NMR signal up to $T_2 \approx 1.5$ μs (2 μs), which limits the maximum temperature of our measurements. Above $T=T_{\text{tp}} \approx 210$ K (T_{tp} means the temperature of transition to a two-phase state) a complex dynamics of nuclear spins, namely, a narrowing of the NMR spectrum when the time interval τ is increased, was detected. As an example, in Fig. 4 we show the spectra at three values of the interval between the exciting and refocusing pulses (see the data for $T=250$ K). This effect is connected with the intrinsic nanoscopic inhomogeneity of the ferromagnetic metallic state in manganites, and has been discussed in detail for

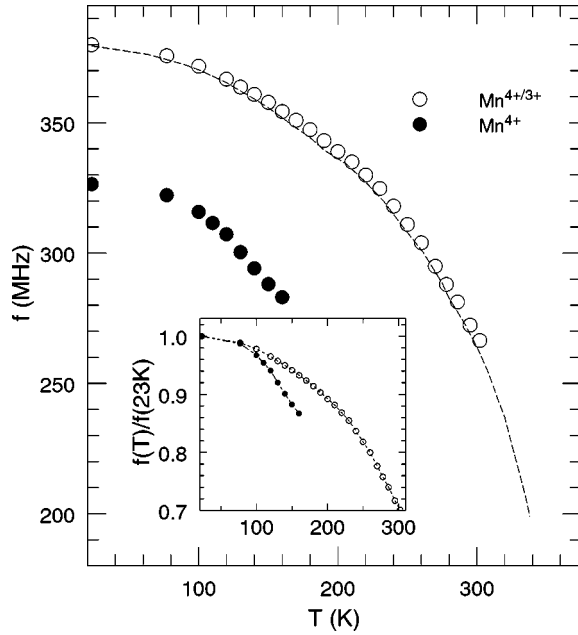


FIG. 5. Temperature dependence of resonance frequencies for $\text{Mn}^{4+/3+}$ (\circ) and Mn^{4+} (\bullet) in a nanosized sample. The dashed curve represents the result for a polycrystalline sample $\text{La}_{0.7}\text{Sr}_{0.3}\text{MnO}_3$ from Ref. 15. Inset: the same dependencies for reduced values.

polycrystalline $\text{La}_{0.7}\text{Sr}_{0.3}\text{MnO}_3$ in Ref. 22. Note that the characteristic dimension of this inhomogeneity was estimated to be a few nanometers.^{22,23} It is not surprising, therefore, that this effect is still observed for particles with the size ~ 50 – 100 nm.

The change of f_{res} with the temperature reflects, according to Eq. (1), the change of the local magnetic moment of $M_{l,i}$ because the hyperfine coupling constant A is temperature independent to a good approximation. The temperature dependence of the NMR frequencies in $\text{La}_{0.7}\text{Sr}_{0.3}\text{MnO}_3$ nanoparticles is shown in Fig. 5 (dots). The dashed curve illustrates the results for a polycrystalline sample of $\text{La}_{0.7}\text{Sr}_{0.3}\text{MnO}_3$ which were taken from Ref. 15. In the inset, for comparison, the temperature dependence of the reduced magnetic moment for the S1 sample and the polycrystalline sample, deduced from NMR and magnetic measurements,¹⁵ is plotted too. We can see for the S1 samples that, in the temperature interval under study, at least for the majority of Mn sites giving rise to the $\text{Mn}^{4+/3+}$ NMR signal, the local magnetic moment of Mn changes with temperature in the same manner as for a polycrystalline compound. This indicates that the double exchange strength in nanoparticle cores is the same as in the bulk material. On the other hand, for Mn^{4+} ions, the NMR frequency and reduced magnetization decrease with temperature much faster (see the full dots on Fig. 5). This implies that, as holes do not visit these sites, this group of sites is under the effect of usual indirect exchange interaction, that is weaker than double exchange and causes different from the bulk magnetic order. The observed NMR temperature dependences do not confirm that the Curie temperature near the grain boundary is enhanced.⁷

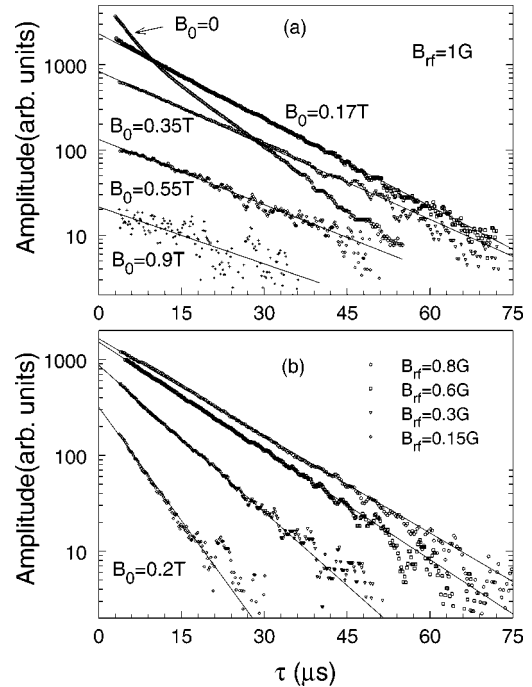


FIG. 6. Nanopowder $\text{La}_{0.7}\text{Sr}_{0.3}\text{MnO}_3$ sample. Spin-echo decay at the maximum of $\text{Mn}^{4+/3+}$ line for five values of the applied magnetic field B_0 at $B_{\text{rf}}=1$ G (a) and for four values of the rf power B_{rf} at $B_0=0.2$ T (b).

B. Spin-spin relaxation

In a ferromagnet, a mixture of NMR signals coming from nuclei in domains and domain walls is usually detected. The nuclei in the domain walls are shown to have a shorter spin-spin relaxation time T_2 than the nuclei in the domains.²⁴ For both our samples, S1 and S2, the decay of the spin-echo amplitude is well described by the sum of two exponential dependences. Moreover, we find that the decay depends on the radio frequency (rf) of the field applied. Note that a similar behavior has also been reported for (La, Na) polycrystals.¹⁷ It is natural therefore to attribute the faster component of the decay rate to the contribution of nuclei in the domain walls, while the slower one is attributed to nuclei in the domains. Since a question may arise as to whether the domain walls still exist for nanoparticles under consideration, we substantiated this attribution by measurements in an applied magnetic field. Indeed, it is seen from Fig. 6(a) that the faster component disappears in a field $B_0 \geq 0.2$ T (at a temperature 77 K), while the slower component survives at higher fields (compare the curves for $B_0=0$ T and for $B_0=0.17$ T). On the other hand, in an applied magnetic field $B_0=0.2$ T the slope of the decay still depends strongly on the rf field used [see the curves in Fig. 6(b)].

Shown in Fig. 7 are the rf field dependences of the amplitudes [Fig. 7(a)] and relaxation times T_2 [Fig. 7(b)] obtained by decomposing the decay recorded in zero external field at $f_{\text{res}}=376$ MHz for two exponentials (for nuclei in the domain with a relaxation time T_2^D , and relaxation time T_2^{DW} for nuclei in the domain wall):

$$A(\tau) = A^D \exp(-2\tau/T_2^D) + A^{DW} \exp(-2\tau/T_2^{DW}).$$

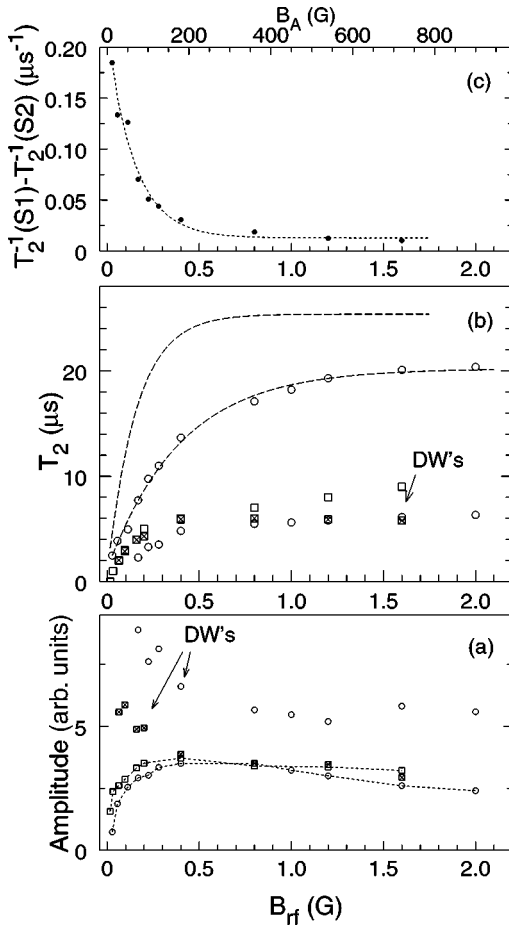


FIG. 7. Amplitude (a) and spin-spin relaxation time T_2 (b) for the domains (slow component of spin-echo decay) and domain walls (faster component of spin-echo decay) in S1 (\circ) and S2 (\diamond) samples. The difference of relaxation rates T_2^{-1} for domain contribution in S1 and S2 samples (c).

The dependence of relaxation time T_2 on the value rf field B_{rf} suggests that there exists a spread of both the relaxation rates and the NMR enhancement factors η in the samples under study—the larger the rf field is, the more nuclear spins with smaller τ and the longer T_2 contributes to the total signal. A similar approach has been successfully applied to explain the NMR in the domain walls of Fe.²⁵ In our case, the intrinsic inhomogeneity of mixed-valency manganites, caused by a random chemical replacement of different size ions, such as La^{3+} and Sr^{2+} , most likely also leads to an inequality of ^{55}Mn nuclei states inside the domains. The different size and form of the grains are also the additional factors that cause the inhomogeneity of internal magnetic field acting on nuclei spins.

The actual field acting on the nuclei consists of the external rf field B_{rf} and the field produced by oscillating magnetic moments of electrons. The presence of the electronic magnetic moments thus enhances the effect of B_{rf} . The corresponding enhancement factor reads,²⁶

$$\eta = B_{hf} / (B_0 + B_A), \quad (2)$$

where the hyperfine field B_{hf} is determined by Eq. (1) and B_A is the magnetic anisotropy field. Experimentally, enhancement factor is related to the values B_{rf}^{opt} of the external rf field, at which the amplitude of the spin echo for the given group of nuclei attains its maximum:

$$\eta^{-1} = 3t(\gamma/2\pi)B_{rf}^{opt},$$

where t is the duration of the rf pulses.

Let us now return to the analysis of the data of Fig. 7 and compare the results for samples S1 and S2. Taking into account broad distribution of optimal resonance conditions for exciting the NMR signal, the amplitudes on Fig. 7(a) should be treated as an average portion of the nuclei for which $B_{rf}^{opt} \approx B_{rf}$. The analysis indicates that in our case for both samples the largest fraction of nuclei in the domains should be excited by large rf fields and the fraction progressively decreases for lower B_{rf} ; most of the nuclei ($>90\%$) are excited by B_{rf} between 0.2 and 2 G ($\eta = 4000 - 400, B_A = 90 - 900$ G).

This analysis may be considered to be a tentative one, as far as the real situation is more complex. In fact we should take into account not only the contributions from nuclei for which B_{rf}^{opt} , but also the non-negligible contributions from nuclei for which $B_{rf}^{opt} \ll B_{rf}$ (“overmodulated” signals). For the same reason the estimation for the fraction of the nuclei in the domain walls is also qualitative. However, it is clear from our results that the contribution of the domain walls signal to the NMR is even larger for nanosized S1 samples [see Fig. 7(a)]. The spin-spin relaxation is faster for S1 samples, especially for the nuclei in the domains. The difference is more pronounced at small rf fields, i.e., when the signal arises from regions with larger η and thus, according to Eq. (2), with a smaller magnetic anisotropy. To demonstrate this fact, the difference of relaxation rates T_2^{-1} for two samples is plotted in Fig. 7(c).

The nuclear spin-spin relaxation in manganites may be explained by fluctuations of the hyperfine field caused by the hopping of electron holes, $T_2^{-1} \sim t_{hop}$, where t_{hop} is the mean correlation time for hopping.¹⁷ The data in Fig. 7 correspond to the maximum of resonance line, where the Suhl-Nakamura (SN) relaxation mechanism arising from indirect spin-spin coupling mediated by virtual spin waves,²⁷ provides an additional contribution to T_2 :

$$T_2^{-1} = T_2^{-1}(hop) + T_2^{-1}(SN).$$

In the wings of the resonance line, however, the SN interaction is ineffective and the relaxation is determined by the $T_2^{-1}(hop)$ contribution only. The values of $T_2^{-1}(hop)$ and $T_2^{-1}(SN)$, obtained from the decays in the wings and maximum of the resonance line for S1 and S2 samples at $B_{rf} = 1$ G, are listed in Table I.

The Suhl-Nakamura contribution $T_2^{-1}(SN)$ to the relaxation rate is the smallest for the nanosized S1 samples. This can be naturally explained because the effectiveness of this mechanism depends on the number of nuclear spins, which precess at or near the given frequency, and this number is reduced with broadening of the NMR line. $T_2^{-1}(hop)$ is

TABLE I. The nuclear relaxation time T_2 parameters.

$T = 77$ K	Domains			Domain walls	
	S1	S2	poly ¹⁵	S1	S2
$T_2^{-1}(\text{hop}), \mu\text{s}^{-1}$	0.034(1)	0.020	0.019	0.120	0.103
$T_2^{-1}(\text{SN}), \mu\text{s}^{-1}$	0.015	0.020	0.022	0.037	0.050

larger in samples S1 compared to $T_2^{-1}(\text{hop})$ for S2 samples implying¹⁷ a slower moving of electron and holes in the nanoparticles. Note that this effect is masked considerably in Fig. 7 due to SN contribution.

The spin-spin relaxation rates T_2^{-1} of the ^{55}Mn in nanosized $\text{La}_{0.7}\text{Sr}_{0.3}\text{MnO}_3$ are shown as a function of temperature in Fig. 8 together with the data for polycrystalline sample (Ref. 15, dashed curve). The rates correspond to the contribution of the nuclei in the domains at a large rf field. Two sets of data for the $\text{Mn}^{4+/3+}$ line at low temperatures are the rates at the center and at the wings of the line. Above $T_{\text{tp}} = 210$ K the rates for slower relaxing part of the spectra are shown. It is seen that the grain size does not appreciably influence the character of the temperature dependence of the relaxation, though the relaxation rate is larger for nanoparticles, as discussed above. The relaxation for the Mn^{4+} line is faster in comparison with the main line relaxation, and this difference increases with increasing temperature. We note that the behavior of the relaxation for Mn^{4+} and $\text{Mn}^{4+/3+}$ lines cannot be explained in the same way. For the $\text{Mn}^{4+/3+}$ line, which corresponds to a fast hopping of electron holes ($f_{\text{hop}} \gg f_{\text{res}}$), the increase of the relaxation rate with temperature implies a slower hopping ($f_{\text{hop}} \rightarrow f_{\text{res}}$) of electron holes due to thermally induced spin disorder (magnetic

polarons).¹⁷ For the Mn^{4+} line ($f_{\text{hop}} < f_{\text{res}}$), if we assume that the spin-spin relaxation is also governed by the fluctuations of the hyperfine field due to the hopping, the increase of the relaxation rate with temperature should then be due to thermally activated hopping. As discussed in detail in Refs. 28 and 29, corresponding centers in ferromagnetic insulating manganites can be viewed as Jahn-Teller small polarons.

V. RESISTANCE AND MAGNETORESISTANCE

To complete our NMR data, we also investigated the resistive and magnetoresistive properties of $\text{La}_{0.7}\text{Sr}_{0.3}\text{MnO}_3$ compacted samples and $\text{La}_{0.7}\text{Sr}_{0.3}\text{MnO}_3/\text{La}_{0.7}\text{Sr}_{0.3}\text{MnO}_3$ junctions as well. Here we briefly discuss these data.

Magnetotransport measurements were performed using the standard four-probe dc method. The samples were prepared by the procedure described in Ref. 9. In particular, a powder plate sized $0.1 \times 1 \times 10 \text{ mm}^3$ was pressed and then subjected to sparing annealing. The reduced temperature and short time of annealing made it possible to prepare plates whose intergrain bonds exhibited the tunneling pattern of current flow. In particular, this was reflected in the observation of a clearly defined low-field magnetoresistive effect. The resistance of initial plates at room temperature was in the range from 2 to 10 Ω . The resistance of current and potential junctions was $R \sim 10^{-7} \Omega \text{ cm}^2$.

First, the temperature dependence of resistance of thus prepared plates of $\text{La}_{0.7}\text{Sr}_{0.3}\text{MnO}_3$ was measured. The latter had a characteristic maximum in the neighborhood of 340 K, associated with the metal-dielectric transition (Fig. 9). The magnetoresistive effect, $[\rho(T,0) - \rho(T,H)]/\rho(T,0)$, in a low magnetic field was also measured; at $T = 77$ K and $H = 100$ Oe, this effect was $\approx 9\%$ (see the inset of Fig. 9).

The procedure for preparing single microcrystal junctions consists of making a ceramic plate of powder glued on an elastic substrate. The substrate is bent until a crack appears in the ceramic plate that passes through all granules in the region of deformation. When the external load is relieved, the plate returns to the initial position, the crack ‘‘closes,’’ and the microcrystals are tightly pressed against one another on the line of break. The most ‘‘correct’’ alignment of the break of microcrystals must be expected to be in a plate region where the shear deformation is minimal. This is apparently one of the reasons why such a procedure results in the realization of only one effective junction of the grain-grain type. In the literature, junctions prepared by a similar procedure came to be known as break junctions (see, e.g., Ref. 9, and references therein). The choice of a single contact with a minimal tunneling resistance from the competing ones is assisted by the very specific nature of the tunneling effect

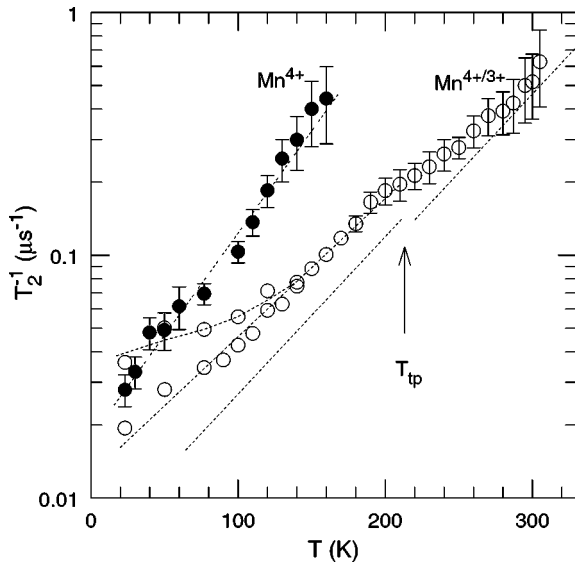


FIG. 8. Temperature dependence of relaxation rates for $\text{Mn}^{4+/3+}$ (\circ) and Mn^{4+} (\bullet) in a nanosized sample. Two sets of data for the $\text{Mn}^{4+/3+}$ line at low temperatures are the rates at the center and at the wings of the line. The dashed curve represents the results for polycrystalline sample $\text{La}_{0.7}\text{Sr}_{0.3}\text{MnO}_3$ from Ref. 21. At low temperatures the rates correspond to the wings of the resonance line.

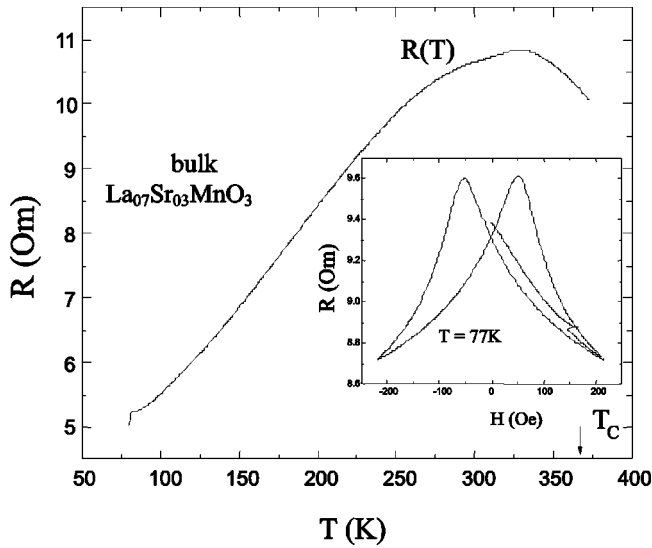


FIG. 9. Temperature dependence of the resistance of compacted nanoparticles plate of $\text{La}_{0.7}\text{Sr}_{0.3}\text{MnO}_3$. The inset gives the magnetoresistive effect, $[\rho(T,0) - \rho(T,H)]/\rho(T,0)$, in a low magnetic field at $T = 77$ K.

in which the value of current depends exponentially on the barrier thickness (a variation of the barrier thickness by 1 Å usually causes a variation of the junction resistance several time over). The small thickness of the plate is an additional important factor in preparing grain-grain junctions.

Figure 10 gives representative behavior of the resistance of $\text{La}_{0.7}\text{Sr}_{0.3}\text{MnO}_3/\text{La}_{0.7}\text{Sr}_{0.3}\text{MnO}_3$ break junction as function of magnetic field at $T = 77$ K; the magnetoresistive effect, $[\rho(T,0) - \rho(T,H)]/\rho(T,0)$, in a low magnetic field; at $T = 77$ K and $H = 100$ Oe, this effect was about 1%.

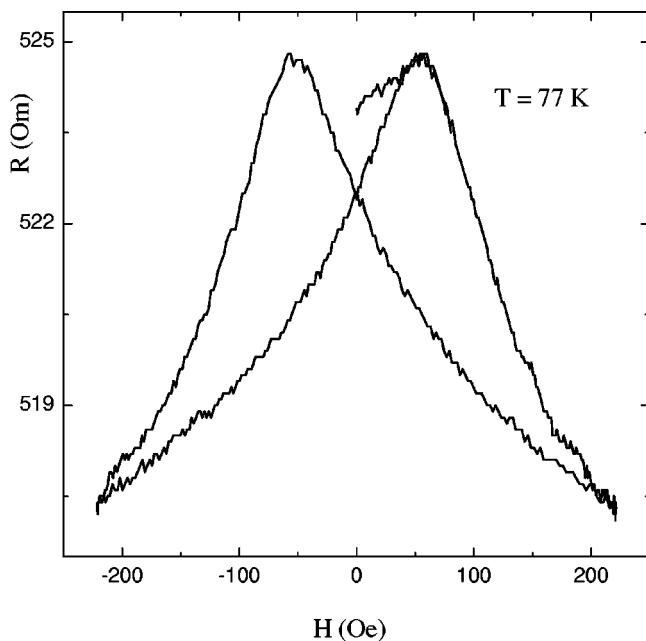


FIG. 10. Magnetoresistive effect of the $\text{La}_{0.7}\text{Sr}_{0.3}\text{MnO}_3/\text{La}_{0.7}\text{Sr}_{0.3}\text{MnO}_3$ junction in low magnetic field at $T = 77$ K.

One can see that in the hysteretic dependence $\rho(H)$ for the bulk sample (Fig. 9) and the tunnel junction (Fig. 10), the maxima of the resistance in magnetic field $H_C \approx 70$ Oe virtually coincide. The hysteresis on the $\rho(H)$ curves is caused by the residual magnetization of microcrystals of the samples, and the field of maximum resistance corresponds to the field of coercivity H_C . Note that for a polycrystalline ceramic sample (large grains) of a similar composition this field was found to be about 30 Oe.⁹

VI. DISCUSSION

Let us first summarize the main features of the ^{55}Mn NMR in the nanoparticles of $\text{La}_{0.7}\text{Sr}_{0.3}\text{MnO}_3$ compared to the bulk material.

(1) The NMR spectra are broader and, in addition to a motional narrowed $\text{Mn}^{4+/3+}$ line, also contain a small contribution arising from Mn^{4+} states localized on the time scale of NMR ($\approx 10^{-9}$ s).

(2) The temperature dependence of the NMR frequency for $\text{Mn}^{4+/3+}$ line and thus the corresponding local magnetic moment of Mn are the same as in the polycrystalline sample of similar composition.

(3) The reduced NMR frequency for the Mn^{4+} line decreases with temperature faster than that for the $\text{Mn}^{4+/3+}$ line, giving a suggestion that the double exchange interaction does not take place for the corresponding Mn^{4+} sites.

(4) Spin-spin relaxation for the $\text{Mn}^{4+/3+}$ line is faster, implying a slower motion of electron holes, especially in the regions with smaller magnetic anisotropy.

The question we have to answer first is: whether these features are really due to the small dimension of the particles under study or are they connected with the inner imperfections of such systems? Indeed, the vacancies in La/Sr sites³⁰ may be considered as a possible source of the NMR broadening. It was documented in Ref. 31 that the linewidth of the motional narrowed line in manganites containing $\sim 30\%$ of Mn^{4+} ions depends on the cation size disorder. The local lattice distortions caused by the vacancies are expected to hinder the hopping of Mn holes and thus should result in both the appearance of the Mn^{4+} NMR line and an increase of the spin-spin relaxation rate. However, the disorder must also influence the Curie temperature strongly, as demonstrated by Rodrigues and Attfield.³² Taking into account the results of recent papers,³¹⁻³³ we estimated that the *observed broadening of the NMR lines has to be accompanied by the decrease of T_C for ~ 40 K if the source of the broadening is the vacancies in La/Sr sites.* Such a possibility can be safely ruled out since according to NMR data the Curie temperature of the nanosized compacted $\text{La}_{0.7}\text{Sr}_{0.3}\text{MnO}_3$ powder does not differ from T_C in the bulk material with an accuracy better than ± 5 K. For this reason we believe that structural disorders, such as the oxygen nonstoichiometry, are not randomly distributed in each particle, but mainly on the grain surface.

This assumption is further confirmed by the electrical data, which support a model of the particles composed of two different parts: an inner core with physical properties similar to the bulk, and an outer shell with oxygen faults, vacancies, etc. Note, that based on the results of magnetic

studies, Zhu *et al.*⁸ and Lopez-Quintela *et al.*,¹² recently proposed a similar structural model for $\text{La}_{2/3}\text{Sr}_{1/3}\text{MnO}_3$ and $\text{La}_{2/3}\text{Ca}_{1/3}\text{MnO}_3$ nanoparticles, respectively. According to this model the core is metallic and ferromagnetic, while the shell is insulating and spin disordering. The results of our careful nuclear spin dynamic investigations can be reasonably fitted to this model. Indeed, the Mn^{4+} line in the NMR spectrum most likely arises from the grain's surface, where holes are localized and the double exchange interaction is replaced by an indirect exchange interaction. The consequent magnetic state possesses a lower ordering temperature and can be totally different from that of the core. The relative fraction of corresponding sites estimated from the integrated area of the NMR signals consists of approximately 3% of total sites. The magnetic properties of the inner part of the particles are essentially the same as in the bulk material, as revealed by the temperature dependence of NMR for $\text{Mn}^{4+/3+}$ line.

In conclusion, we have presented detailed studies of the

^{55}Mn NMR spectra and a nuclear relaxation study of half-metallic $\text{La}_{0.7}\text{Sr}_{0.3}\text{MnO}_3$ nanoparticles. It was found that the magnetism of the surface boundary is significantly different from that of the particle bulk. The surface magnetic (dis)order progressively decreases from the surface to the inner part of the particles with non-negligible consequences for nuclear spin dynamics, connected with the electron-hole hopping. However, in the inner part of the particles the strength of the double exchange interaction is preserved. Electrical transport properties support the model. These results are of great relevance for spin-electronic devices based on an exploration of the nanoscale magnetism of manganites and their half-metallic features.

ACKNOWLEDGMENTS

The authors are very grateful to Marec Maryshko for a valuable SQUID analysis of the samples, and to Valentine Doroshev for helpful discussions.

-
- ¹N. Zhang, W. Ding, W. Zhong, D. Xing, and Y. Du, *Phys. Rev. B* **56**, 8138 (1997).
- ²J.-H. Park, E. Vescovo, H.-J. Kim, C. Kwon, R. Ramesh, and T. Venkatesan, *Phys. Rev. Lett.* **81**, 1953 (1998).
- ³K. Steenbeck, T. Eick, K. Kirsch, H.-G. Schmidt, and E. Steinbeiss, *Appl. Phys. Lett.* **73**, 2506 (2001).
- ⁴J. E. Evetts, M. G. Blamire, N. D. Mathur, S. R. Isaac, B.-S. Teo, L. F. Cohen, and J. L. Macmanus-Driscoll, *Philos. Trans. R. Soc. London, Ser. A* **356**, 1593 (1998).
- ⁵M. Ziese, *Phys. Rev.* **60**, 738(R) (1999).
- ⁶R. Gross, L. Alff, B. Büchner, B. H. Freitag, C. Höfener, J. Klien, Y. Lu, W. Mader, J. B. Philipp, M. S. R. Rao, P. Reutler, S. Ritter, S. Thienhaus, S. Uhlenbruck, and B. Wiedenhorst, *J. Magn. Magn. Mater.* **211**, 150 (2000).
- ⁷Y.-A. Soh, G. Aeppli, N. D. Mathur, and M. G. Blamire, *Phys. Rev. B* **63**, 020402(R) (2000).
- ⁸T. Zhu, B. G. Shen, J. R. Sun, H. W. Zhao, and W. S. Zhan, *Appl. Phys. Lett.* **78**, 3863 (2001).
- ⁹V. Yu. Tarenkov, A. I. D'yachenko, and V. N. Krivoruchko, *Zh. Eksp. Teor. Fiz.* **120**, 205 (2001) [*JETP* **93**, 180 (2001)].
- ¹⁰A. Glaser and M. Ziese, *Phys. Rev. B* **66**, 094422 (2002).
- ¹¹M. Ziese, *Rep. Prog. Phys.* **65**, 143 (2002).
- ¹²M. A. Lopez-Quintela, L. E. Hueso, J. Rivas, and F. Rivadulla, *Nanotechnology* **14**, 212 (2003).
- ¹³M. Bibes, Ll. Balcells, S. Valencia, J. Fontcuberta, M. Wojcik, E. Jedryka, and S. Nadolski, *Phys. Rev. Lett.* **87**, 067210 (2001).
- ¹⁴T. E. Konstantinova, I. A. Danilenko, N. P. Pilipenko, and G. K. Volkova, in *Proceedings of the International Symposium "Solid Oxide Fuel Cells VIII,"* edited by S. C. Singhal and M. Dokiya, Electrochemical Society Proceedings Vol. 2003-07 (2003), p. 153.
- ¹⁵P. Novak, M. Marysko, M. M. Savosta, and A. N. Ulyanov, *Phys. Rev. B* **60**, 6655 (1999).
- ¹⁶G. J. Chen, Y. H. Chang, and H. W. Hsu, *J. Magn. Magn. Mater.* **219**, 317 (2000).
- ¹⁷M. M. Savosta, V. A. Borodin, and P. Novak, *Phys. Rev. B* **59**, 8778 (1999).
- ¹⁸J.-P. Renard and A. Anane, *Mater. Sci. Eng., B* **63**, 22 (1999).
- ¹⁹Cz. Kapusta, P. C. Riedi, W. Kocemba, M. R. Ibarra, and J. M. D. Coey, *J. Appl. Phys.* **87**, 7121 (2000).
- ²⁰G. Allodi, M. Cestelli Guidi, R. De Renzi, and M. W. Pieper, *J. Magn. Magn. Mater.* **242-245**, 635 (2002).
- ²¹M. M. Savosta and P. Novak, *J. Magn. Magn. Mater.* **242-245**, 672 (2002).
- ²²M. M. Savosta and P. Novak, *Phys. Rev. Lett.* **87**, 137204 (2001).
- ²³R. H. Heffner, J. E. Sonier, D. E. MacLaughlin, G. J. Neieuwenhuys, G. Ehlers, F. Mezei, S.-W. Cheong, J. S. Gardner, and H. Roder, *Phys. Rev. Lett.* **85**, 3285 (2000).
- ²⁴I. D. Weisman, L. J. Swartzendruber, and L. H. Bennett, in *Technique of Metal Research*, edited by E. Passaglia (Wiley, New York, 1973), Vol. VI.
- ²⁵M. B. Stearns, *Phys. Rev.* **187**, 648 (1969).
- ²⁶E. A. Turov and M. P. Petrov, *Nuclear Magnetic Resonance in Ferro- and Antiferromagnets* (Halsted, New York, 1972).
- ²⁷J. H. Davis and C. W. Searle, *Phys. Rev. B* **9**, 323 (1974).
- ²⁸G. Allodi, M. C. Guidi, R. De Renzi, A. Caneiro, and L. Pinsard, *Phys. Rev. Lett.* **87**, 127206 (2001).
- ²⁹M. M. Savosta, V. I. Kamenev, V. A. Borodin, P. Novak, M. Marysko, J. Hejtmanek, K. Dorr, and M. Sahana, *Phys. Rev. B* **67**, 094403 (2003).
- ³⁰G. Dezanneau, A. Sin, H. Roussel, H. Vincent, and M. Audier, *Solid State Commun.* **121**, 133 (2002).
- ³¹M. M. Savosta, P. Novak, Z. Jirak, J. Hejtmanek, and M. Marysko, *Phys. Rev. Lett.* **79**, 4278 (1997).
- ³²L. M. Rodriguez and J. P. Attfield, *Phys. Rev. B* **54**, R15 622 (1996).
- ³³M. M. Savosta, A. N. Ulyanov, N. Yu. Starostyuk, M. Marysko, and P. Novak, *Eur. Phys. J. B* **12**, 393 (1999).